J. Fluid Mech. (1988), *vol.* 191, *pp.* 111–135
Printed in Great Britain

Asymptotic intensity of the quasi-periodic oscillations in fully developed turbulent shear layers

By ANUVAT SIRIVAT
Department of Mechanical Engineering, University of Pittsburgh, Pittsburgh, PA 15261, USA

(Received 2 January 1986 and in revised form 1 September 1987)

Turbulent shear layers generated from a common splitter plate as well as from a half-frame screen are investigated experimentally in the developing regime and in the asymptotic regime. The phase-averaged means with time delay of velocity fluctuations are analysed in terms of Fourier modes in the frequency domain to give both the amplitude and frequency of the local fundamental mode due to the presence of the large-scale organized motion. The amplitudes of both the streamwise and the transverse components tend to relax to asymptotic values that are independent of the velocity ratio as well as the shear-layer apparatus. The Strouhal number St, defined as fL/U_a, where f is the local fundamental mode frequency, L is the shear-layer width and U_a, is the average convection velocity of the structures is found to be initially dependent on the local Reynolds number. In the asymptotic regime, the orientation of the large-scale structures is tilted backward toward the higher-speed side in all cases.

1. Introduction

Turbulent shear-layer flow has been extensively studied by numerous investigators. The early experimental study of Liepman & Laufer (1947) showed that both mean and fluctuating velocity profiles are nearly self-preserving. The turbulent kinetic energy and the zone-averaged statistics based on the intermittency function were studied in detail by Wygnanski & Fiedler (1970). Their work has been followed by Spencer & Jones (1971), Jones, Planchon & Hemmersley (1973), Patel (1973) and more recently Champagne, Pao & Wygnanski (1975). All these works were primarily focused on statistical descriptions of the flow such as the linear growth rate and the self-preserving profiles of various velocity fluctuation statistics.

Brown & Roshko (1974) and Winant & Browand (1974) demonstrated the existence of a large-scale vortex structure in turbulent shear layers at high and moderate Reynolds numbers respectively, mainly by flow visualization techniques. Subsequent works on the large-scale structure were by Browand & Weidman (1975), Dimotakis & Brown (1976), Koochesfahani *et al.* (1979), Wygnanski *et al.* (1979), Browand & Troutt (1980) and Jimenez (1983, 1985). They showed that these structures are visible and measurable near the origin of the flow. It is known now that they are responsible for the growth of the shear-layer width by means of vortex pairing and/or the increase in their sizes, as they are convected downstream.

On the other hand, Pui & Gartshore (1979) and Chandrasuda *et al.* (1978) suggested that the nearly two-dimensional large-scale structures observed are rare; they can occur only in favourable conditions such as low free-stream turbulent intensity or

laminar boundary layers at the splitter plate. Batt (1977) reported that no periodicity was found or could be identified from the spectra in his fully developed shear layer.

In addition to the study of the large-scale structure characteristics embedded in a turbulent shear layer, some parallel studies were aimed at understanding the effects of initial and boundary conditions on the velocity profiles in the self-preserving state. These studies include Batt (1975), Hussain & Zedan (1978*a*, *b*), Browand & Latigo (1979) and most recently Dziomba & Fiedler (1985). They have shown that the state of the boundary layers at the splitter plate is critical in the development of the self-preserving state of the shear layer. Further studies of a shear layer subjected to artificial disturbances near the origin have been undertaken by Ho & Huerrre (1984), Oster & Wygnanski (1981), Dziomba & Fiedler (1985) and more recently Gaster, Kit & Wygnanski (1985). They suggested that the external periodic disturbances can control, in a particular region, the shear-layer growth rate, turbulent intensities and the large-scale structure interactions depending upon the frequency and the amplitude used.

Previously, the large-scale structures have been indirectly linked to the extremely sensitive initial conditions of the shear layer and found to be relatively weak and to contribute a negligibly small fraction of the turbulent kinetic energy (Wygnanski *et al.* 1979). In order for these structures to be dynamically significant, they must play a major role in turbulent momentum transport (Hussain 1983). On the other hand, Dimotakis & Brown (1976) showed that these structures are responsible for strong periodic velocity fluctuations, noticeably near the shear-layer edges. At present, no measurement of the large-scale motions 'within' the fully developed shear layer has been reported, when the flow visualization techniques fail to identify them.

In the present study, we are interested in identifying the presence and the relative strength of the large-scale organized structures in the developing regime and in the asymptotic regime when they evolve naturally without the presence of any artificial forcing.

2. Experimental apparatus and instrumentation

The wind tunnel is a closed-return type as used previously by Comte-Bellot & Corrsin (1966, 1971). The test section, located after the secondary contraction (ratio 1.27:1) has a 1.22 m × 0.91 m cross-section and it is 9.5 m in length.

Two methods of generating shear layers were used in the present investigation. A thin aluminium splitter plate 122 cm wide, 50 cm long and 0.206 cm thick was located after the secondary contraction at the tunnel mid-height. To provide a differential pressure drop between the top and bottom flow channels, a single screen frame was mounted on top of the splitter plate and a set of three screens was attached on the bottom side (figure 1). The screens were made of stainless steel with diameter of 1.905 mm and a spacing of 24 meshes per inch, giving a geometric solidity ratio of 0.33. The screens also served as means of smoothing any disturbances created by the plate leading edge upstream and reducing the plate boundary-layer thickness downstream. A set of steel wires, with a diameter of 0.55 mm, were used to keep the splitter front end from possible vibrations and sagging.

For the second method of generating a shear layer the splitter and the set of screens were replaced with a single half-frame screen. The location of this half-frame screen is shown in figure 1. The stainless steel screen used was 2.79 mm in diameter, with a spacing of 30 per inch and a geometric solidity ratio of 0.55 in order to provide

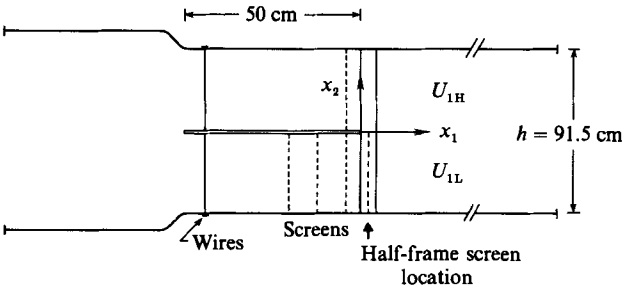

FIGURE 1. The test section of the wind tunnel showing the splitter plate and the location of the half-frame screen.

a sufficient differential pressure drop. The residue velocity fluctuations generated from this above the critical value of the screen solidity were measured to be negligibly small in the region far downstream in excess of 5000 screen meshes (the laboratory coordinates of the half-frame screen experiments to be described below are taken to be at the location of the screen). At and beyond this distance downstream, the mean transverse velocity component measured was found to be nearly zero. It appeared that the deflected mean streamlines had become nearly parallel again at and beyond $x_1 = 2.0$ m. This is in agreement with a recent study by Oguchi & Inoue (1984) who showed that both mean and fluctuating profiles of the shear layer generated from a half-frame screen achieve a self-preserving state not far downstream.

All measurements of the mean streamwise velocity component were done by a Pitot-static tube and a micromanometer. All velocity fluctuations were measured with constant-temperature hot-wire anemometers (DISA type 55D01), operated at an overheat ratio of 0.6. The transverse and the streamwise components of velocity fluctuations within the shear layer were measured with a symmetric X-array meter (DISA 55P51), made of two gold-plated tungsten wires 5 μm in diameter and 1.25 mm in sensitive wire length, giving a length-to-length ratio of 250. The minimum Kolmogorov microscale was estimated from the balance between the turbulence production term and the dissipation term to be about 0.1 mm (for the half-frame screen experiment with $\Delta U = 7.08$ m/s). This gives a minimum value of the microscale–wire-length ratio of about 0.1. The value is rather low for the study of small-scale fluctuations; however, it should be adequate in measurements of the large-scale properties such as energy and cross-correlation. No wire-length corrections were applied to the present data. The signals from the X-array meter were low-pass filtered at 5 kHz (DISA type 55D25) prior to digitization. The maximum Kolmogorov frequency was estimated at the shear-layer centreline to be about 16 kHz. The energy loss due to the analog filtering, however, was found to be negligible in any of the experiment runs. Repeated measurements of r.m.s. values from 20 records, each record spanning 50–200 integral timescales, showed scatter within a few percent. Independent measurements using a single hot wire and an r.m.s. voltmeter agreed with the above digitized data, also within a few percent. Two single hot wires were positioned outside the shear layer and used as reference signals. The velocity signals at these positions monitored irrotational velocity fluctuations, mainly due to the passage of the large-scale structures. These reference signals were filtered at about 150 Hz, without losing relevant information. The traversing mechanism for the X-array meter is accurate to within 0.2 mm.

	Half-frame screen experiments		Splitter-plate experiments		
$\bar{U}_{1H}$	14.6	9.71	12.1	14.7	11.9
$\bar{U}_{1L}$ (m/s)	7.52	4.66	8.8	10.7	7.30
Velocity difference $\Delta U \equiv \bar{U}_{1H} - \bar{U}_{1L}$ (m/s)	7.08	5.05	3.30	4.00	4.60
Velocity ratios $r \equiv \dfrac{\bar{U}_{1L}}{\bar{U}_{1H}}$	0.52	0.48	0.73	0.73	0.61
$R \equiv \dfrac{\bar{U}_{1L} - \bar{U}_{1L}}{\bar{U}_{1H} + \bar{U}_{1L}}$	0.32	0.35	0.16	0.16	0.24
Growth rate $\dfrac{dL}{dX_1}$	0.536	0.0510	0.0269	0.0322	0.0406
Virtual origin x_0 (m)	0.533	0.197	−1.84	−1.84	−1.84

TABLE 1. Shear-layer experiment parameters

Data acquisition was done using a microcomputer (IBM PC) with a fast A/D converter (Techmar) having a 12 bit resolution. Digitized data were stored on streaming tapes and could be later restored for analysis. All computations and analysis were done on this microcomputer. Some plots were done on the mainframe computer (VAX 780) graphic utility.

3. Experimental results: time-averaged statistics

A summary of the flow parameters investigated is given in table 1. The first measurement of each experiment run was to determine the shear-layer width as a function of the distance downstream and its growth rate. The mean streamwise component of velocity was measured with the Pitot-static tube and a micromanometer. The mean velocity $\bar{U}_1$ is normalized with $\bar{U}_{1L}$ and $\Delta U = \bar{U}_{1H} - \bar{U}_{1L}$ as $U^* = (\bar{U}_1 - \bar{U}_{1L})/\Delta U$, where $\bar{U}_{1H}$ and $\bar{U}_{1L}$ are the mean free-stream velocity on the high-speed side and the low-speed side respectively. The shear-layer width L at a given x_1/h, where x_1 is the streamwise laboratory coordinate and h is the tunnel height, is defined to be the transverse distance between x_{2H} and x_{2L} where U^* is equal to 0.9 and 0.1 respectively. The dimensionless transverse coordinate η is defined as $(x_2 - x_{2c})/L$, where x_{2c} is the locus of $U^* = 0.5$.

Figure 2(*a*) shows loci of x_{2H}, x_{2L} and x_{2c} for the splitter-plate experiments for various ΔU and velocity ratios $r = \bar{U}_{1L}/\bar{U}_{1H}$. The growth of the shear-layer width L is approximately linear from $x_1/h > 1.5$ up to $x_1/h = 7$. Here the streamwise and the transverse coordinates x_1 and x_2 are normalized with h, the tunnel height, in order to show the relative extent of the shear-layer width and the tunnel width. In all cases, L/h is never above 0.4 at the last measurement station. For a fixed $r = 0.73$, there is a slight difference in the shear-layer-width growth rate when ΔU is increased from 3.3 m/s to 4.0 m/s. This is unexpected since dL/dx_1 should be proportional to $R \equiv \Delta U/(\bar{U}_{1H} + \bar{U}_{1L})$ (Brown & Roshko 1974). For both cases, the loci of x_{2H} and x_{2c} are nearly the same. The difference is on the lower-speed side where the spread of the shear-layer width is faster for the case of higher ΔU or higher $U_a = \frac{1}{2}(\bar{U}_{1H} + \bar{U}_{1L})$. For the flow where $r = 0.61$, the locus of x_{2c} appears to deviate from the splitter-plate plane, as one would expect for a shear layer with a lower r or higher R.

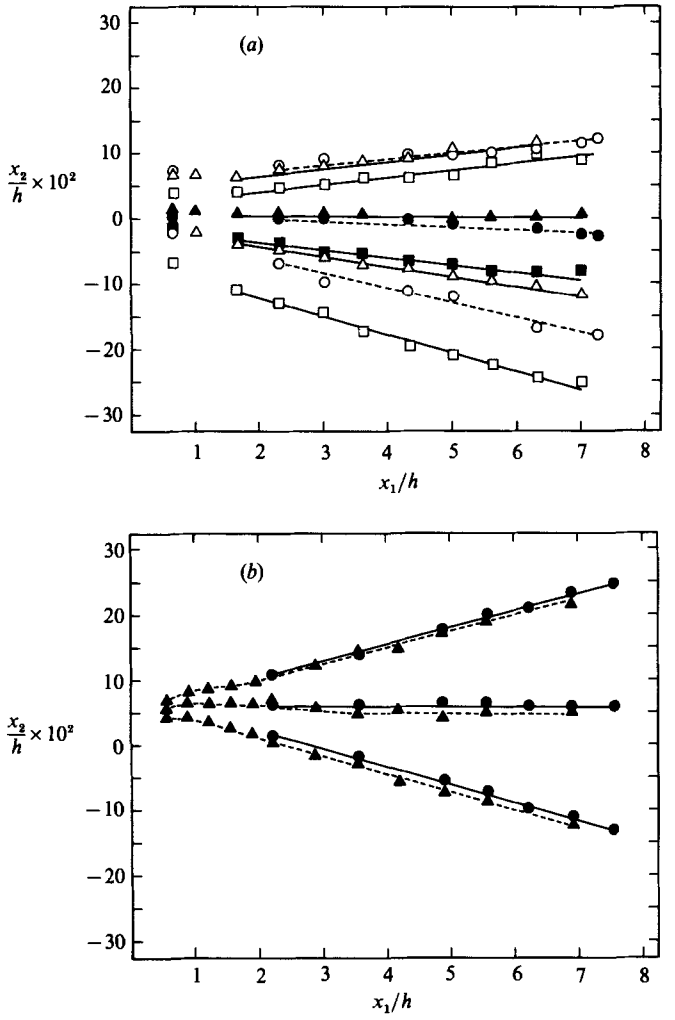

FIGURE 2. The growth of the shear-layer width. (*a*) Splitter-plate experiments with solid symbols representing the loci of $\eta = 0$: ○, $\Delta U = 4.0$ m/s; △, 3.3 m/s; □, 4.6 m/s. (*b*) Half-frame-screen experiments: ●, $\Delta U = 7.08$ m/s; ▲, 5.05 m/s. The tunnel height h is 91.5 cm.

For the half-screen experiments, the shear-layer width grows linearly after about $x_1/h = 2.0$ up to about $x_1/h = 7$ (figure 2*b*). The spread of the shear-layer widths on the lower-speed side and on the higher-speed side are nearly equal and are less sensitive to changes in U_a for a fixed r or R compared with the splitter-plate experiments above. In both types of shear-layer apparatus, the velocity difference between the high and low speeds was varied by merely changing the incoming uniform flow speed without an appreciable change in R or r. The velocity ratio r was varied by adding or removing an additional screen in the case of the splitter-plate experiment. For the half-frame-screen experiment, r was found to be nearly fixed for a given screen, depending mainly on the differential pressure drop.

The normalized mean velocity profiles, plotted with the dimensionless coordinate η are nearly self-preserving, at least in the region where the shear-layer growth is linear. Figure 3 shows the normalized mean velocity profiles for both the splitter plate and the half-frame screen with $\Delta U = 4.6$ m/s and 7.08 m/s respectively. Both

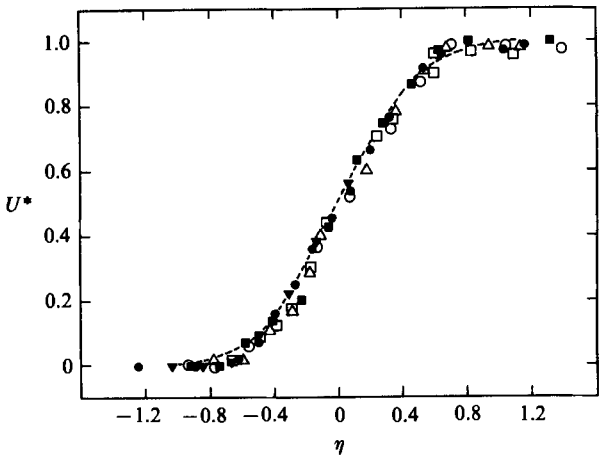

FIGURE 3. The non-dimensional mean velocity profiles. Splitter-plate experiments, $\Delta U = 4.6$ m/s; ○, $x_1 = 3.94$ m; △, 5.16 m; □, 6.38 m. Half-frame-screen experiments, $\Delta U = 7.08$ m/s: ■, $x_1 = 3.27$ m; ●, 4.48 m; ▼, 5.70 m. The dashed line is the curve $(\frac{1}{2}(1+\mathrm{erf}(a\eta)$, $a = 1.82$.

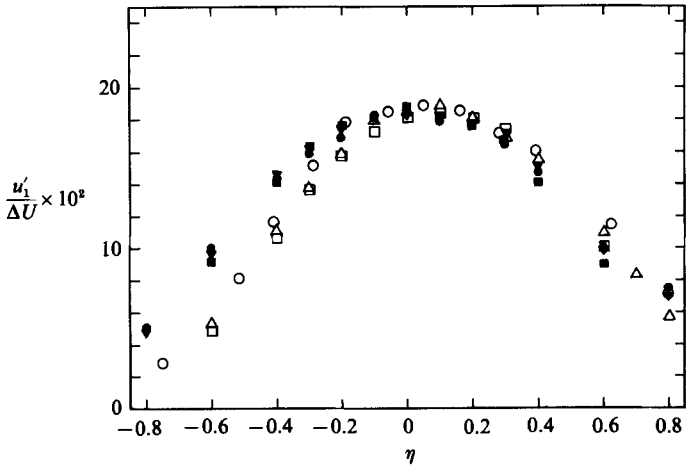

FIGURE 4. The streamwise component turbulent intensity profiles. The splitter-plate experiment, $\Delta U = 4.6$ m/s, $r = 0.61$, $R = 0.24$: ○, $x_1 = 3.23$ m; △, 4.45 m; □, 5.76 m. The half-frame-screen experiment, $\Delta U = 7.08$ m/s, $r = 0.52$, $R = 0.32$: ●, $x_1 = 2.55$ m; ▼, 3.77 m; ■, 6.82 m.

the self-preserving profiles could be approximated by an error function of the type $U^* = \frac{1}{2}(1+\mathrm{erf}(a\eta))$, where $a = 1.82$ (Townsend 1976; Pui & Gartshore 1979). In the regions outside the turbulent shear layer, the mean velocity profiles are uniform within experimental accuracy, except near the walls. In all the experiment runs, no increase in the $\bar{U}_{1H}$ or $\bar{U}_{1L}$ was found with distance downstream. This might have been caused by the growth of the boundary layers at the walls. Thus, no wall adjustment was required for each experiment.

Figure 4 compares the streamwise turbulent intensity profiles for both the splitter-plate and the half-screen experiments in the self-preserving region. The noticeable difference is the distribution of profiles on the lower-speed side, where the profiles for the splitter-plate experiment are slightly skew. The reason for this is unclear. However, the maximum intensity occurs at about the centreline and is approxi-

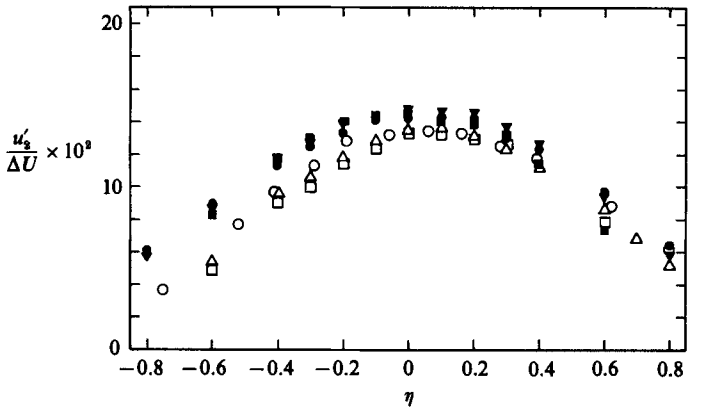

FIGURE 5. The transverse component turbulent intensity profiles. The flows and the symbols are the same as in figure 4.

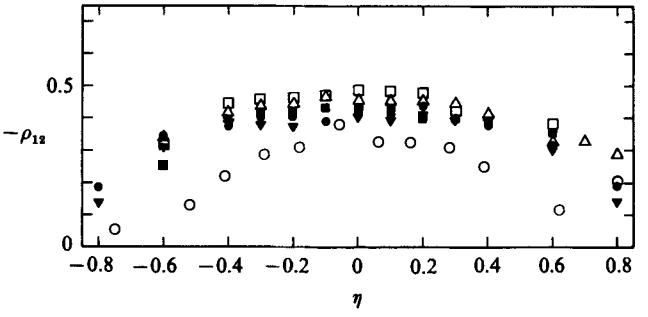

FIGURE 6. The cross-correlation profiles. The flows and the symbols are the same as in figure 4.

mately equal to 0.19 for both experiments despite the difference in R. Figure 5 shows the corresponding transverse turbulent intensity profiles where the profiles for the half-screen experiments are nearly everywhere larger than the splitter-plate experiment. The latter experiment has a maximum of 13.5, compared to the value of 14.5 for the former experiment. Finally, the profiles of ρ_{12} are compared in figure 6. A similarity between both experiments is the nearly uniform value of ρ_{12} near the centreline, extending approximately from $\eta = -4$ to $+0.4$ with a maximum value of about -0.45. The splitter-experiment profile, however, is lower near the origin ($x_1 = 3.23$ m). At this measuring station, both of the fluctuating velocity intensities are self-preserving (figures 4 and 5). Figure 7 (a, b) shows the development of the turbulent intensities for both components plotted in terms of the streamwise coordinate $x_1 - x_0$, where x_0 is the virtual origin. Only the flows of $\Delta U = 7.08$ m/s and 4.60 m/s are self-preserving as shown in figure 7 (a). Other flows reported here are still in the development state within the streamwise extent of measurement. All the shear layers generated from the splitter-plate experiments reported here appear to originate from initially laminar boundary layers. The peaks in the $u_1'/\Delta U$ profiles first increase to their maximum values followed by gradual drops toward their values in the self-preserving state (Hussain & Zedan 1978a, b). On the other hand, for the shear layer generated from the half-frame screen, the peaks in the $u_1'/\Delta U$ profiles increase monotonically toward the self-preservation value, which is nearly identical to the splitter plate experiment at $R = 0.32$. This behaviour is similar to the splitter-

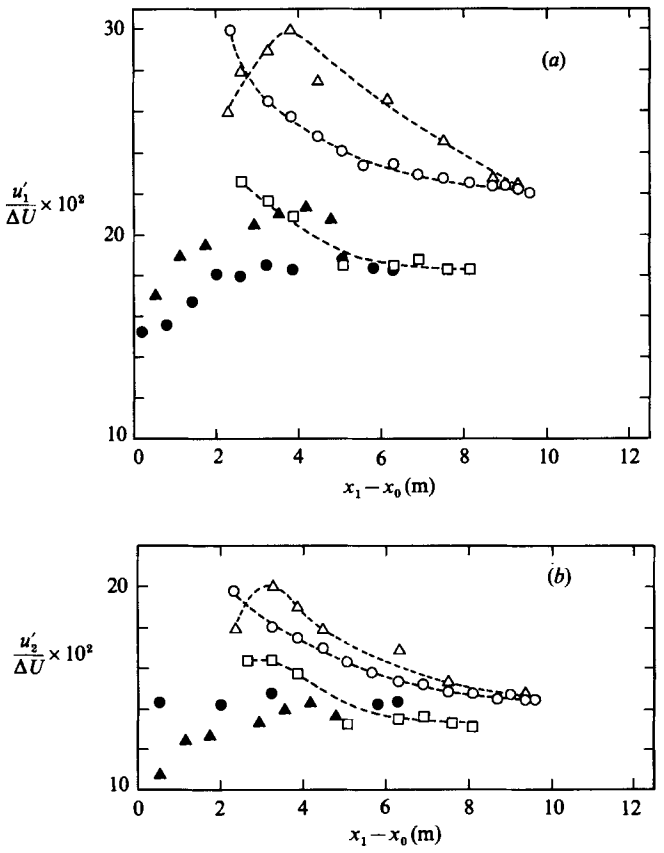

FIGURE 7. Development of the turbulent intensities at the shear-layer centrelines, $\eta = 0$. Splitter-plate experiments: △, $\Delta U = 3.3$ m/s; ○, 4.0 m/s; □, 4.6 m/s. Half-frame-screen experiments: ●, $\Delta U = 7.08$ m/s; ▲, 5.05 m/s. (*a*) $u_1'/\Delta U$; (*b*) $u_2'/\Delta U$.

plate experiments with initially turbulent boundary layers (Browand & Latigo 1979; Dziomba & Fiedler 1985). However, the half-frame-screen apparatus itself generates no boundary layer whether laminar or turbulent. Thus the initial conditions, such as the state of the initial boundary layer at the splitter-plate trailing edge or the initial Reynolds number *Re* based on momentum thickness, do not alone play a direct role in the present half-frame-screen experiments. The streamwise velocity fluctuations r.m.s. peak values are extremely sensitive to the initial conditions and relax slowly toward the self-preservation state. The transverse component r.m.s. peak values, shown in figure 7 (*b*), are much less dependent on the initial conditions. They relax to the asymptotic value of about 0.14, regardless of the means of flow-generating devices and the velocity ratios.

4. Detection of the large-scale structure

4.1. *Previous studies*

The existence of large-scale vortical motion in the shear layer originating from a splitter plate has been observed using flow visualization techniques by Brown & Roshko (1974) and Winant & Browand (1974). Closer to the origin, where the vortices are nearly two-dimensional and small-scale fluctuations are not yet set in,

the motion of the large-scale structures may be readily inferred from a dominant peak of the velocity spectrum. Detailed measurements and analysis of laminar-shear-layer instabilities have been given by Freymuth (1966), Winant & Browand (1974) and later by Miksad (1972, 1973). The generation of subharmonic disturbances is now known to be associated with pairing between adjacent vortices. Further downstream, these large-scale structures are subjected to other instability modes such as helical pairing (Chandrsuda *et al.* 1978), multiple pairing forming a cluster of vortices (Ho & Huang 1981) or partial pairing (Hussain 1983). As a result, small-scale fluctuations set in and the velocity spectrum appears as a broad-band turbulence signal.

There are several approaches to detecting the large-scale structures that are embedded in fully developed turbulence. Townsend (1976) measured spatial-correlation functions to infer the structure shape and size. A similar approach has been followed by Tavoularis & Corrsin (1981) and Mumford (1982). A somewhat more systematic approach is the orthogonal decomposition. Payne & Lumley (1966) successfully used Grant's data of a cylinder wake to infer the large-scale structure as counter-rotating eddies in pairs. Another technique, phase averaging, has been successful in revealing the large-scale structure when the flow is periodic with known period (Hussain & Reynolds 1971; Cantwell & Coles 1983) or when the flow is forced at a frequency corresponding to the local unstable disturbance (Oster & Wygnanski 1982). For natural or unforced flow, the passage of the large-scale structure is usually inferred from the nearly periodic velocity fluctuations outside the turbulent zone. Koochesfahani *et al.* (1979) were able to measure the circulation associated with the vortices within a shear layer. Winant & Browand (1974) and later Browand & Weidman (1975) used reference signals coupled with the flow visualization to obtain the phase-averaged velocity fields in moderate-Reynolds-number shear layers. Hussain (1983) reported several techniques used in a fully developed turbulent jet.

4.2. *A physical model of a large-scale structure*

To detect the arrival time of a single isolated large-scale structure within the fully developed shear layer, a physical model is needed in place of the flow visualization. Figure 8 depicts a single isolated plane vortex with its centre located at a displacement c above a fixed coordinate $\boldsymbol{x}$, from an array of randomly positioned plane vortices. The interfaces of the turbulent shear layer or the superlayers (Corrsin & Kistler 1955) on the high- and low-speed sides are at τ_{H} and τ_{L} from the structure centre respectively. Outside the superlayer boundaries, the motions can be assumed to be irrotational. Each superlayer that separates the turbulent zone from the irrotational zone is at any instant in general very irregular but continuous. The irrotational motion, however, depends only on the transverse velocity component at the interface (Phillips 1955). In the figure are shown the prescribed transverse velocity distributions at the two superlayers that would be caused by the presence of a large-scale vortical structure. Both reference frames $\boldsymbol{y}$ and $\boldsymbol{y}'$ are assumed to move at the structure convection velocity U_{c}. The equation of motion in the irrotational zone and the corresponding boundary conditions on the high-speed side are

$$\nabla^2\phi_{\mathrm{H}}(\boldsymbol{y}) = 0, \tag{1}$$

$$\phi_{\mathrm{H}} \to 0, \quad y_2 \to \infty, \tag{2a}$$

and

$$v_{2\mathrm{H}}(y_2 = 0) = \frac{\partial \phi_{\mathrm{H}}}{\partial y_2} = A_{\mathrm{H}} \sin(k_1 y_1 + k_3 y_3 + \psi_{\mathrm{H}}). \tag{2b}$$

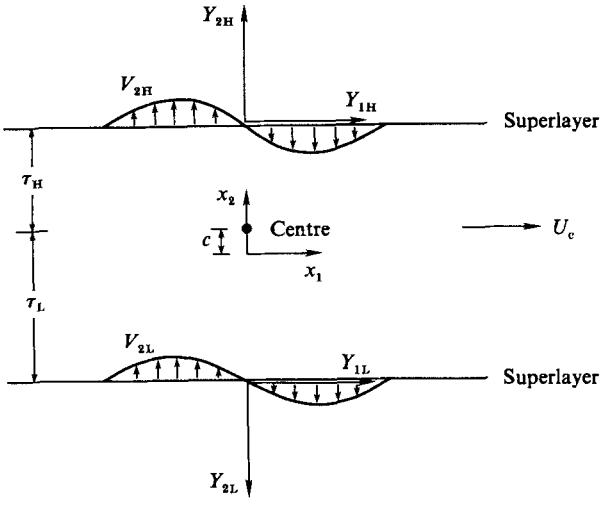

FIGURE 8. A physical model of the large-scale structure showing the velocity distributions at the two superlayers.

The fixed phase ψ_H of the high-speed-side velocity distribution is π. The solution of the above equation satisfying the boundary conditions is

$$\phi_H(y) = -\frac{A_H}{k} e^{-ky_2} \sin(k_1 y_1 + k_3 y_3 + \psi_H). \tag{3}$$

k is the magnitude of a wave vector $\boldsymbol{k}$. The corresponding streamwise velocity in the moving frame $\boldsymbol{y}$ is

$$v_{1H}(y) = -\frac{k_1 A_H}{k} e^{-ky_2} \sin(k_1 y_1 + k_3 y_3 + \psi_H), \tag{4}$$

valid for $y_2 \geqslant 0$. The coordinate transformations from the moving frame to a fixed laboratory frame are

$$y_1 = x_1 - U_c t, \quad y_2 = (x_2 - c) - \tau_H, \quad y_3 = x_3.$$

At $t = 0$, both frames coincide in the streamwise coordinate.

Using the above coordinate transformations, the streamwise velocity fluctuation is

$$u_{1H}(x,t) = -\frac{k_1 A_H}{k} e^{k(\tau_H + c)} e^{-kx_2} \sin(k_1 x_1 + k_3 x_3 + \psi_H - \omega t), \tag{5}$$

where $\omega = k_1 U_c$ is the oscillation frequency and $\psi_H = \pi$.

The same analysis can be extended to the irrotational motion on the low-speed side. The result is

$$u_{1L}(x,t) = -\frac{k_1}{k} A_L e^{k(\tau_L - c)} e^{kx_2} \sin(k_1 x_1 - k_3 x_3 - \omega t + \psi_L). \tag{6}$$

The relations above are valid for $(x_2 - c) \geqslant \tau_H$ and $(x_2 + c) \leqslant -\tau_L$ respectively, where τ_H and τ_L are always positive definite. c is the structure vertical offset from the shear-layer centreline where $\bar{U}_1 = \frac{1}{2}(\bar{U}_{1H} + \bar{U}_{1L})$. ψ_L is identically equal to zero as a result of the velocity distribution on the low-speed side.

For an array of the large-scale structures randomly positioned in the moving

frame, the generalization of the result would be $\psi_H = \pi + \phi(t)$ and $\psi_L = \phi(t)$, where $\phi(t)$ is the time-dependent phase jitter associated with the random spacing between adjacent vortices. Thus both u_{1H} and u_{1L} are quasi-periodic in time in the fixed frame with random amplitudes proportional to $A_H\, e^{k\tau_H}$ and $A_L\, e^{k\tau_L}$ and with dependence on the transverse coordinate as $e^{-k|x_2|}$. The crucial feature of the model is that u_{1H} and u_{1L} obtained from the two fixed probes will be nearly 180° out of phase (as shown also by Winant & Browand 1974). The departure from this phase relationship would be expected since the structure shape is distorted as a result of the strain field, inducing more complicated boundary conditions than previously assumed in (2*b*).

4.3. *Experimental set-up*

At a given distance downstream, two single hot wires were located at between $\eta = 1.1$ and 1.3 and at between $\eta = -1.1$ and -1.3. The hot-wire axes were aligned perpendicular to the interfaces and the mean flow so that they were sensitive only to the streamwise velocity fluctuations, which presumably were due to the irrotational motions caused by the passage of the splitter-plate structures. At these positions, the intermittency was close to zero, as checked visually on the oscilloscope during data acquisition and later from the spectral analysis.

Within the turbulent zone, the velocity fluctuations of both components were measured with a single X-array meter, positioned in the same plane and at the same streamwise coordinate as the reference probes. A tranversing mechanism allowed detailed measurement at various η-coordinates. To minimize possible probe holder feedback effects, all the probes were positioned approximately 50 cm upstream from the tranversing mechanism. No appreciable difference in results was found when the tranversing mechanism was moved ± 10 cm relative to the probe streamwise coordinate.

4.4. *Computations and phase alignment*

The period of the arrival time of the large-scale vortices was estimated from the peaks of the spectra of the streamwise velocity fluctuations of the reference probes located outside the turbulent zone. In nearly all the cases, the spectrum peaks occurred at the same frequency for both the high- and low-speed sides of the shear layer. If there was a measurable difference, the average value of the two was taken. The data sampling rate was then set so that there were at least 32–64 sampled data points in the period. This limited the phase resolution to between 5° and 10°. For a given record size, too fast sampling would reduce the number of the structure ensembles. At each measurement location, a data set consisted of 20 block of data, each block containing 4 records spanning 2^{11} points of about 50 integral time-scales. All velocity fluctuation moments computed here were found to be accurate to within a few percent.

The arrival time of the large-scale structure was chosen to be the instant that reference signals reached a maximum and a minimum on the high- and low-speed sides respectively. The amplitude thresholds were varied from $u_{1H} > 0.6, u_{1L} < -0.6$ to $u_{1H} > 1.2, u_{2L} < -1.2$. A phase delay between the maximum and the minimum of $\pm 30°$ was allowed. The use of two simultaneous reference signals was necessary to differentiate between a single isolated structure and a pair of structures in the fusion or pairing process (Winant & Browand 1974). The single isolated structure would correspond to about 180° phase delay between u_{1H} and u_{1L}, whereas a pair of structures would destroy the phase relationship. For each data block, the arrival time set $t_j, j = 1, N$ was obtained from the above conditions. The variations of the

amplitude thresholds and the phase delay within the above limits only reduced or increased the number of realizations. No significant difference in the ensemble-averaged properties was found.

A component of velocity fluctuation is defined as the sum of the large-scale and the random motions, i.e.

$$u_\alpha(\boldsymbol{x},t) = u_{c\alpha}(\boldsymbol{x},t)+u_{r\alpha}(\boldsymbol{x},t). \tag{7}$$

Then the phase average of (7) is (Hussain 1983)

$$\langle u_\alpha(\boldsymbol{x},t)\rangle = \langle u_{c\alpha}(\boldsymbol{x},t)\rangle, \tag{8}$$

where by definition $\langle u_{r\alpha}(\boldsymbol{x},t)\rangle = 0$. The difference between each realization and the ensemble mean is

$$u_\alpha(\boldsymbol{x},t)-\langle u_\alpha(\boldsymbol{x},t)\rangle = u_{q\alpha}(\boldsymbol{x},t)+u_{r\alpha}(\boldsymbol{x},t), \tag{9}$$

where $u_{q\alpha}(\boldsymbol{x},t) = u_{c\alpha}(\boldsymbol{x},t)-\langle u_{c\alpha}(\boldsymbol{x},t)\rangle$. The present definition distinguishes clearly between the fluctuations of each realization of the large-scale motion from its ensemble mean and the purely random motion. The necessity for this definition is clear when considering the time-averaged turbulent kinetic energy $\overline{u_\alpha^2}$, i.e.

$$\overline{u_\alpha^2(x,t)} = \overline{\langle u_{c\alpha}\rangle^2}+\overline{u_{q\alpha}^2}+\overline{u_{r\alpha}^2}, \tag{10}$$

which assumes that $u_{r\alpha}$ is uncorrelated with either $\langle u_{c\alpha}\rangle$ or $u_{q\alpha}$ and $\overline{u_{q\alpha}\langle u_{c\alpha}\rangle} = 0$. The contribution to the total turbulent kinetic energy from the large-scale structures consists then of two parts, the ensemble mean part and the quasi-random part. For periodic flow, $u_{q\alpha}$ is zero by definition.

The physical origins of $u_{q\alpha}$ are that structures may have many degrees of freedom such as the strength, the structure orientation, the centre offset c, the structure size and modulation in the spanwise direction. The estimate of the magnitude of $\overline{u_{q\alpha}^2}$, however, depends not only on the conditions used in the ensemble averaging but also on additional assumptions such as whether $u_{r\alpha}$ can be regarded as a purely stationary time series, i.e. $\overline{u_{r\alpha}^2} = \langle u_{r\alpha}^2\rangle$. Near the origin, where each structure is in the developing state with a limited number of degrees of freedom, the quasi-random part may be negligibly small in comparison with the purely random part. In most fully developed turbulent flows, the term may contain a considerable fraction of the total turbulent kinetic energy.

In addition to the many degrees of freedom of the evolving structure, there is also the problem of the uncertainty in detecting the arrival time of the structure centre. This arises because, although the reference probes are located locally, their instantaneous responses to the presence of the structure are nonlinear. This is also a well-known problem when a reference probe is located at the origin and the arrival time downstream is estimated from the average convection speed. To remedy this, the arrival times were corrected by successive ensemble-averaging and cross-correlation (Sokolov *et al.* 1980). The procedure consisted of obtaining a zeroth-order ensemble-averaged mean with time delay of the streamwise velocity fluctuations using the arrival time set obtained from the reference signals according to the conditions above. For each realization, a cross-correlation was computed with the ensemble-averaged mean. The time Δt_j was located where the cross-correlation function was at positive maximum. The new arrival time was then $t_j+\Delta t_j, j = 1, N$. The first-order ensemble-averaged mean was then computed from this new arrival time set. The procedure was repeated until no appreciable change in the ensemble-averaged mean could be achieved or no further phase alignment was possible. Only

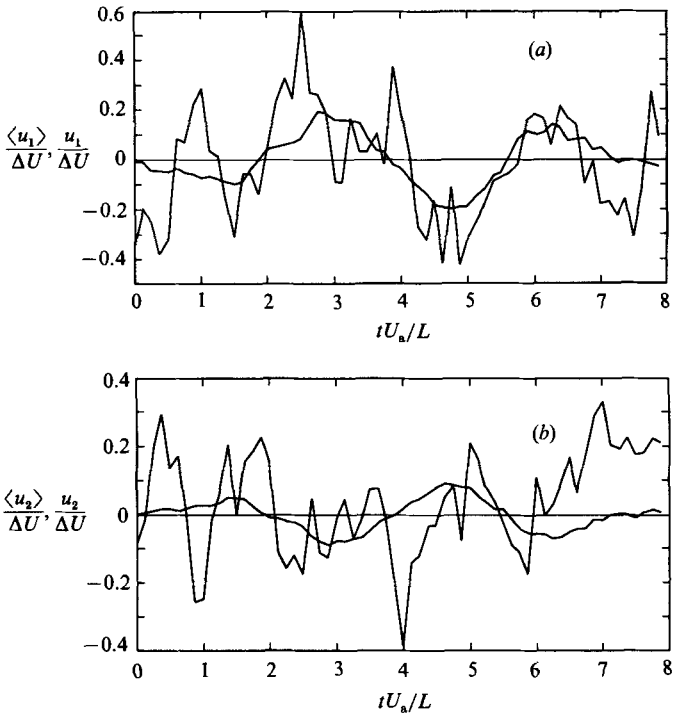

FIGURE 9. Ensemble-averaged means of velocity fluctuations of the splitter-plate experiment, $\Delta U = 4.0$ m/s, $\eta = 0$ and $x_1 = 3.23$ m. Typical realizations of the ensembles are superimposed. (*a*) Streamwise component; (*b*) transverse component.

2–4 iterations were found to be sufficient for the present phase resolution. No digital filtering was applied to the data in the phase alignment process. The number of ensembles used in averaging varied between 300 and 500. No significant difference was found in the ensemble-averaged mean when using up to 800 realizations. The final arrival time set obtained from the ensemble-averaged mean of the streamwise velocity fluctuations at each measurement position was then used in all subsequent ensemble averaging of other turbulent properties.

5. Experimental results: phase-averaged properties

5.1. *Phase-averaged means*

The ensemble-averaged means with time delay of the streamwise and transverse velocity fluctuations are shown in figures 9(*a*, *b*) with typical realizations superimposed. The immediate observation is that for the realization in figure 9(*a*), the instantaneous u_1 shows a similar pattern to its ensemble mean. For the transverse component, the ensemble-averaged mean and the realization are much less similar. A possible explanation for this is that the large-scale structure consists of a large number of vortex sheets which have been rolled up. Only the transverse velocity fluctuations are more indicative and appear as large and random spikes. However, the ensemble-averaged means of both components are comparable in magnitude.

Figures 10 and 11 show the ensemble-averaged means of both the velocity components and the vector plots in the (x_2, t)-plane of the shear layers generated from the splitter plate and the half-frame screen respectively. The velocity patterns

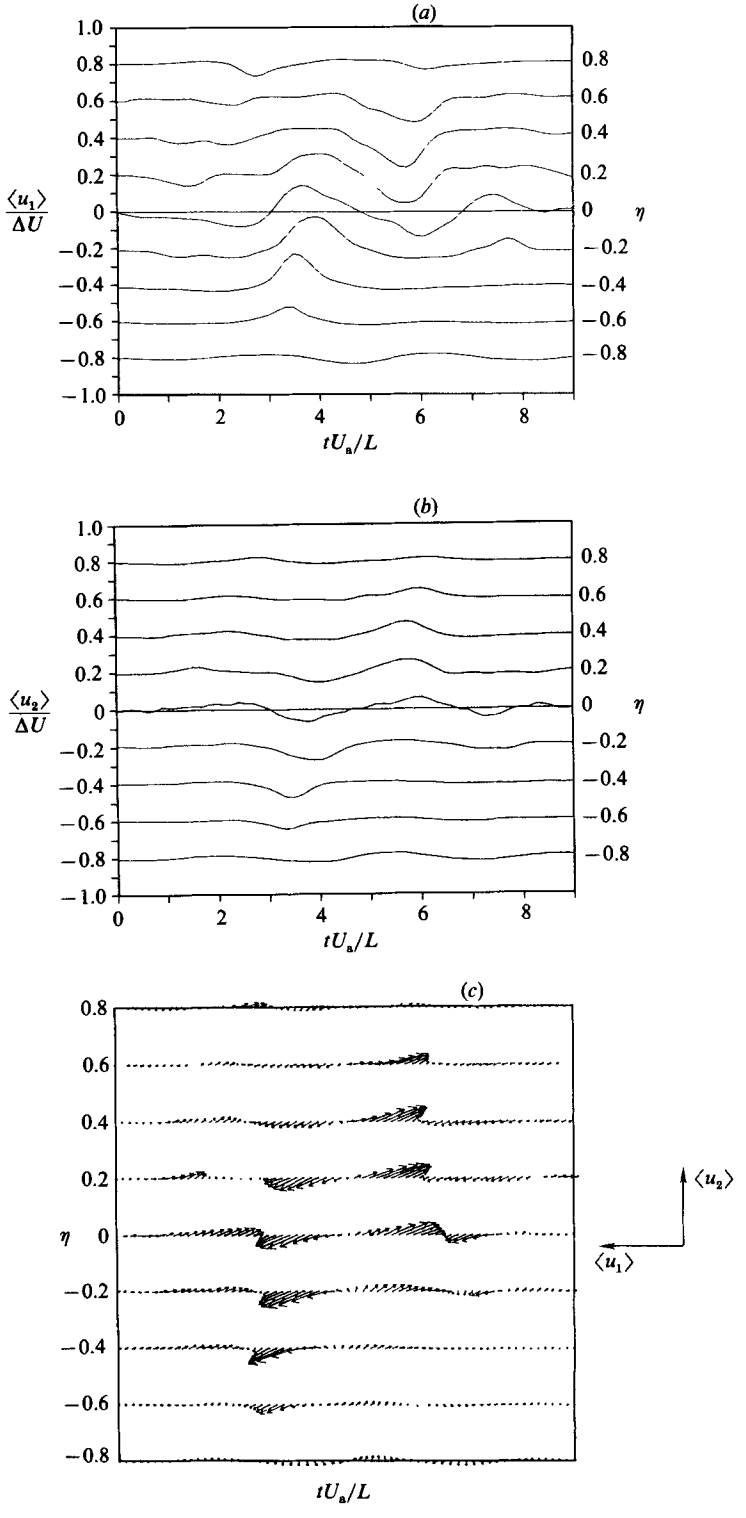

FIGURE 10. The ensemble-averaged means of velocity fluctuations across the shear-layer width, the splitter-plate experiment, $\Delta U = 4.0$ m/s, $x_1 = 5.66$ m. (*a*) Streamwise component; (*b*) transverse component; (*c*) vector plot.

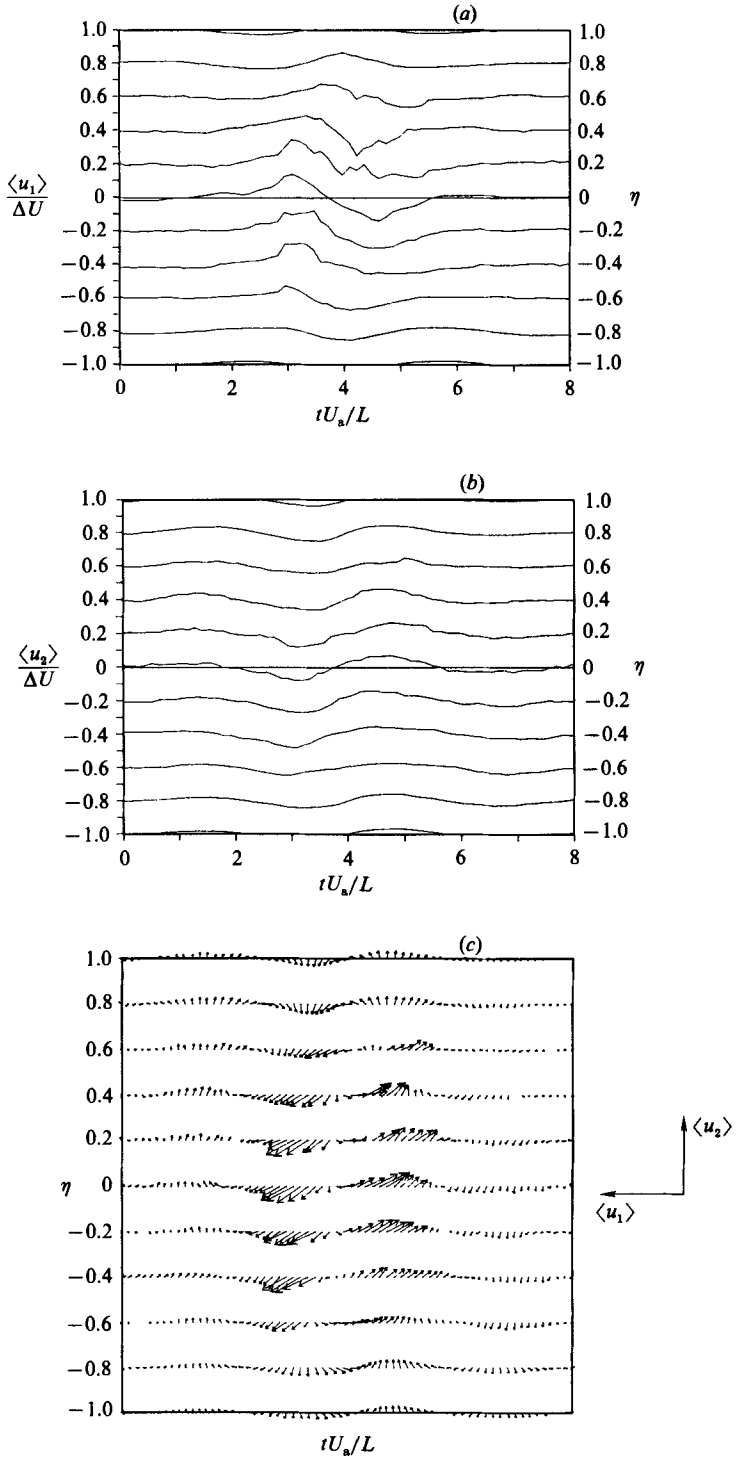

FIGURE 11. The ensemble-averaged means of velocity fluctuations across the shear-layer width, the half-frame-screen experiment, $\Delta U = 7.08$ m/s, $x_1 = 3.77$ m. (*a*) Streamwise component; (*b*) transverse component; (*c*) vector plot.

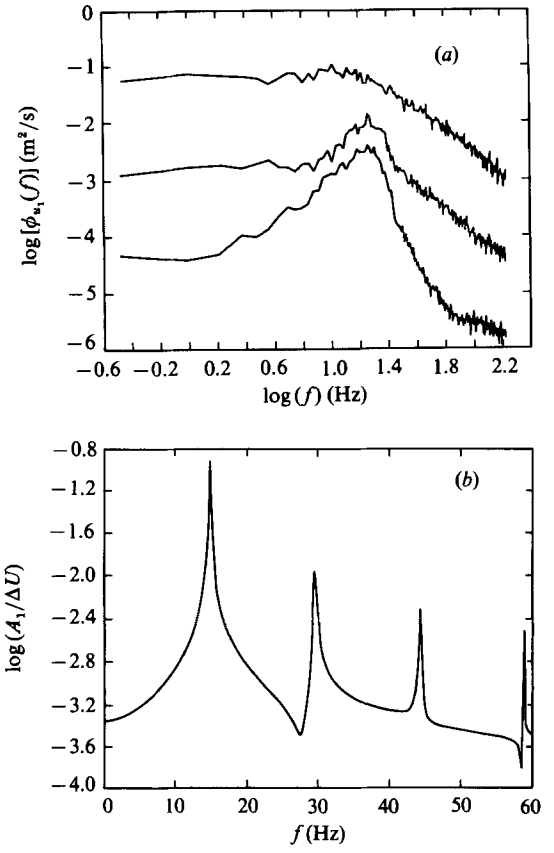

FIGURE 12. (*a*) Spectra of streamwise velocity fluctuations of the half-frame-screen experiment, $\Delta U = 7.08$ m/s, $x_1 = 3.16$ m at $\eta = -0.24$, -0.87 and -1.28 from the top to the bottom of the figure respectively. (*b*) Fourier amplitude of the ensemble-averaged mean of the streamwise velocity fluctuations at $\eta = 0$, half-frame-screen experiment, $\Delta U = 7.08$ m/s and $x_1 = 3.77$ m (figure 11*b*).

are similar in appearance. Both the strength of the structure measured by the amplitude and the phase relationships between the velocity components are nearly the same.

The arrival time of the phase point corresponds to the mid-points of the normalized timescale for both figures. At this phase, the ensemble-averaged or the phase-averaged means of the streamwise velocity fluctuations show a maximum and a minimum at the high- and low-speed sides respectively (figures 10*a* and 11*a*). As a consequence, there is a continuous phase shift of nearly 180° across the shear-layer width. The mean positions of the interfaces of the turbulent shear layer can be taken to be at $\eta = 0.5$ and -0.5. For the transverse velocity component, the ensemble-averaged means are shown in figures 10(*b*) and 11(*b*). A nearly zero or small phase shift of the transverse velocity ensemble-averaged means is found across the shear-layer width. However, the phase differences between the two velocity components at the shear-layer edges (in the irrotational zone) are found to be about 90°. The expected values were 180°, according to the physical model shown in figure 8. All the phase distributions of both velocity components and the relative phase across the shear layer suggest that the large-scale motion is not unlike the simple physical

model, despite the fact that the instantaneous responses between the structure and the irrotational motions across the interfaces are nonlinear. The velocity vector plots (figures 10*c* and 11*c*) also reveal that the shape of the large-scale structure is not circular as in the simplified model, but tilting backward on the high-speed side.

From the ensemble-averaged mean fields shown, both velocity components of the large-scale motions appear to be periodic in time with decaying amplitudes about the arrival time or the phase point. The period of the ensemble-averaged means is estimated to be independent of the time delay as well as the transverse coordinate η, for a fixed downstream distance. In fact, this is nearly the same as the average period inferred from the peak of the streamwise-velocity-fluctuation spectrum obtained in the irrotational zone. Figure 12(*a*) shows spectra of the streamwise velocity fluctuations at three transverse positions. Only the peak of the spectrum for the motions outside the shear layer can be identified with the passage frequency of the structure within the shear layer. The finding that the amplitudes of the ensemble-averaged means decay with the time delay is a result of the randomly arriving time, not an experimental artifact.

5.2. *Analysis of data*

A realization of $u_{c\alpha}(\boldsymbol{x}, t)$ defined in (7) can be expressed in terms of the usual Fourier series

$$u_{c\alpha}(\boldsymbol{x}, t) = \sum_{\omega^k} A_\alpha(\omega^k) \cos(\omega^k t + \phi_\alpha(\omega^k, t) + \psi_\alpha^k), \tag{11}$$

where ω^k is the oscillation frequency and ψ_α^k and $\phi_\alpha(\omega^k, t)$ are the fixed phase and the phase jitter for each oscillation mode. The ensemble-averaged mean or the phase-averaged mean of $u_{c\alpha}(\boldsymbol{x}, t+\tau)$, where τ is the time delay, is

$$\langle u_{c\alpha}(\boldsymbol{x}, t+\tau)\rangle = \sum_{\omega^k} \langle A_\alpha^k \cos(\omega^k(t+\tau) + \phi_\alpha(\omega^k, t+\tau) + \psi_\alpha^k)\rangle. \tag{12}$$

The t corresponds to an arrival time of each structure or to a constant phase of the fundamental mode, i.e. $t = C_\alpha^0 - \psi_\alpha^0 + \phi_\alpha^0(t)/\omega^0$, where $C_\alpha^0 =$ constant. At these instants, other mode phases,

$$C_\alpha^k(t) = \omega^k t + \phi_\alpha^k(t) + \psi_\alpha^k$$

may assume any particular values, since ω^k is not restricted to be rational with the fundamental ω^0, and no probability density function of ϕ_α^k is known. As a result of the large numbers of realizations used in the ensemble-averaging, it can be expected that

$$\langle \cos(\omega^k(t+\tau) + \phi_\alpha^k(t+\tau) + \psi_\alpha^k)\rangle$$

must be zero for any $\omega^k \neq \omega^0$ and at any τ including 0. Thus the ensemble-averaged mean at a constant phase of a mode rejects other modes whose phases do not have any statistical correlation with the phase of the fundamental mode:

$$\langle u_{c\alpha}(\boldsymbol{x}, t+\tau)\rangle = \langle A_\alpha \cos(\omega(t+\tau) + \phi_\alpha(t+\tau) + \psi_\alpha)\rangle. \tag{13}$$

The superscript 0 of the fundamental mode has been dropped from the above expression and omitted in the following discussions. However, the above arguments do not imply that other modes of oscillation due to the large-scale motions are unimportant or can be ignored.

To show the effects of the phase jitter, one may assume that A_α and $\phi_\alpha(t)$ are uncorrelated at any $t+\tau$, and $\phi_\alpha(t+\tau)$ and $\phi_\alpha(t)$ are jointly normal random stationary

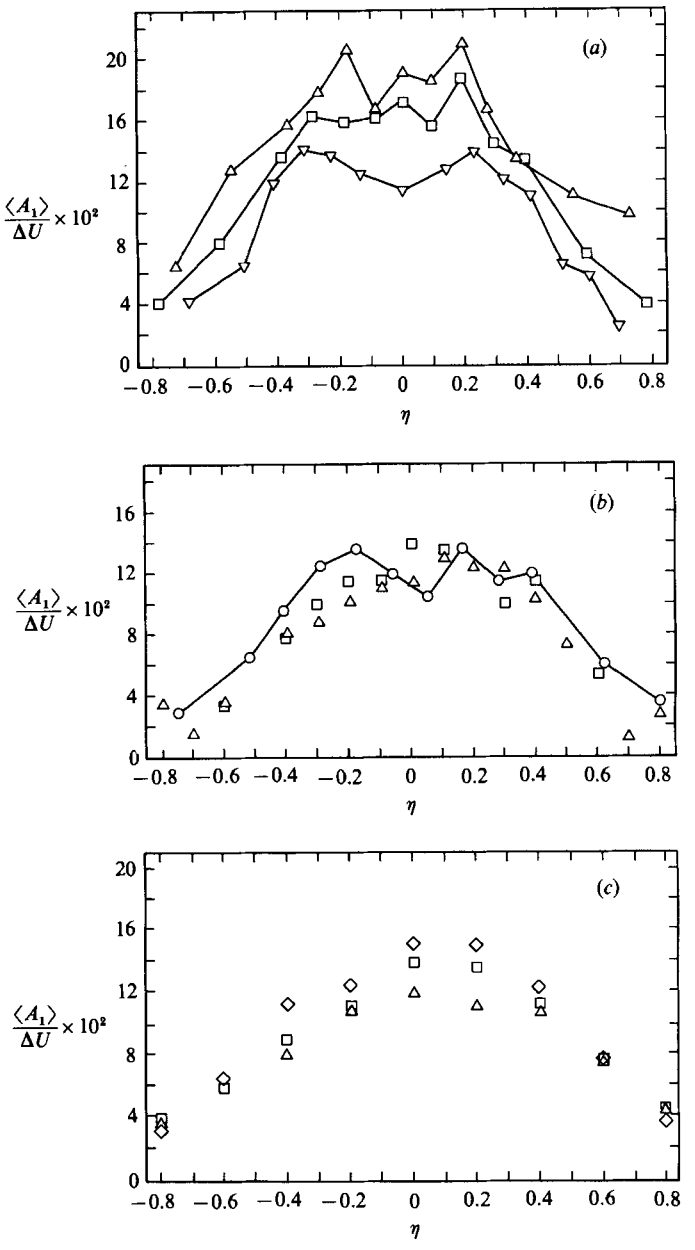

FIGURE 13. The development of the amplitude profiles for the streamwise component. (*a*) The splitter-plate experiment in the developing state, $\Delta U = 3.3$ m/s: △, $x_1 = 2.62$ m; □, 5.67 m; ▽, 7.50 m. (*b*) The splitter-plate experiment in the self-preservation state, $\Delta U = 4.6$ m/s: ○, $x_1 = 3.23$ m; △, 4.39 m; □, $x_1 = 5.67$ m. (*c*) The half-frame-screen experiment in the self-preservation state, $\Delta U = 7.08$ m/s: △, $x_1 = 3.17$ m; □, 4.38 m; ◇, 5.60 m.

process with zero means. The first assumption implies that the strength of each structure and its arrival time are uncorrelated. The second assumption asserts that the random displacement of each structure from its equilibrium position is a normal process. With the above assumptions, the relation (13) reduces to

$$\langle u_{c\alpha}(\boldsymbol{x}, t+\tau) \rangle = \langle A_\alpha \rangle \exp[-\tfrac{1}{2}\sigma^2_{\Delta\phi_\alpha}] \cos[C_\alpha + \omega\tau]. \tag{14}$$

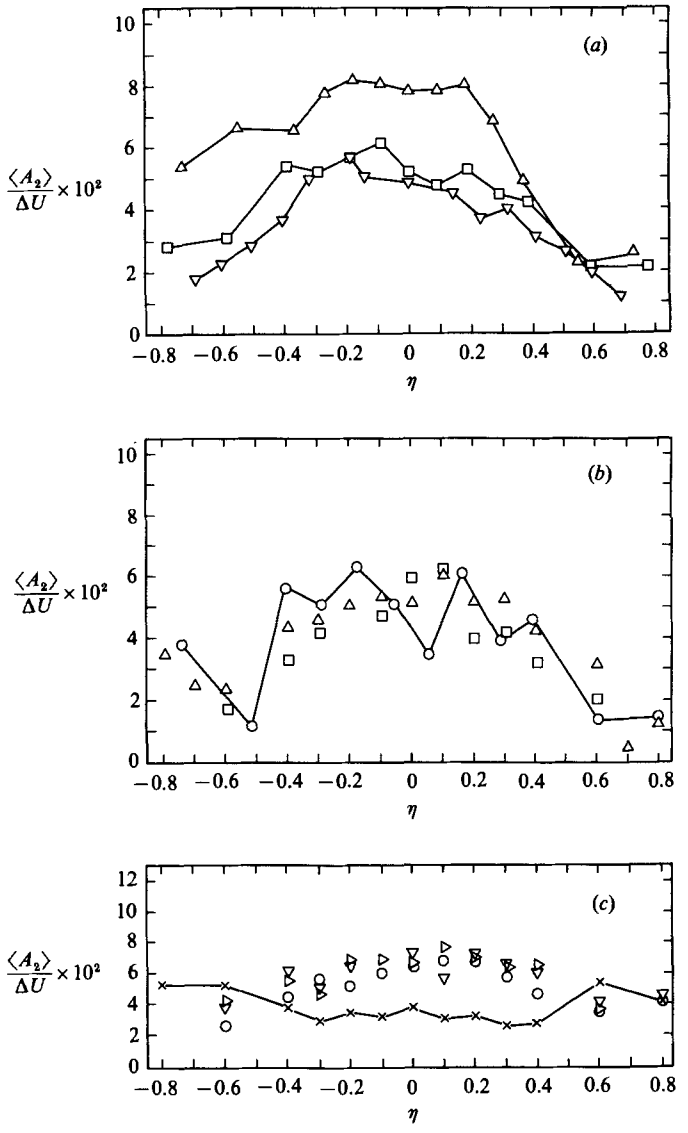

FIGURE 14. The development of the amplitude profiles for the transverse component. The symbols are the same as in figure 13 except in (*c*): ×, $x_1 = 1.02$ m; ○, 2.55 m; ▽, 3.77 m; ▽, 6.82 m.

For a given downstream position, A_α, $\Delta\phi_\alpha = \phi_\alpha(t+\tau) - \phi_\alpha(t)$ and C_α are functions of η, in general. $\Delta\phi_\alpha$ is independent of t and $\sigma^2_{\Delta\phi_\alpha}$ is the variance of $\Delta\phi_\alpha$. At the origin $\tau = 0$, the decaying factor $\exp[-\frac{1}{2}\sigma^2_{\Delta\phi_\alpha}]$ is unity. For a long time delay with $\phi_\alpha(t)$ having a finite integral scale, $\langle \Delta\phi^2_\alpha \rangle \to 2\langle \phi^2_\alpha \rangle$ and the factor $\exp[-\frac{1}{2}\sigma^2_{\Delta\phi_\alpha}]$ approaches a non-zero finite value. This value is, however, small enough to be comparable with the experimental accuracy. The representation in (14) is in qualitative agreement with the experimental results shown in figures 10 and 11.

It is also possible to estimate the amplitude and frequency of the phased-averaged means by Fourier analysis in the frequency domain. First, the phased-averaged mean $\langle u_\alpha(\boldsymbol{x}, t+\tau) \rangle$ was truncated to only $-\pi \leqslant \omega\tau < \pi$ where $\exp[-\frac{1}{2}\sigma^2_{\Delta\phi_\alpha}]$ was still close to unity and where ω, estimated from the time interval between peaks of the

phase-averaged mean at $\eta = 0$, was the fundamental frequency. The total ensemble-averaged mean was reconstructed to be periodic using the truncated $\langle u_\alpha(\boldsymbol{x}, t+\tau)\rangle$, spanning about 40–60 periods depending upon the sample rate. The long record is needed to minimize the leakage reduction in the fast Fourier transform (Bendat & Piersol 1971). Figure 12(*b*) shows the oscillation amplitude as a function of frequency. The peak corresponds to the fundamental amplitude $\langle A_\alpha\rangle$. The magnitude of the harmonics and other background modes are found to be relatively small and negligible in comparison. Periodically, the oscillation amplitude was also estimated by graphical means. The results were essentially the same.

5.3. *Amplitude profiles and evolution*

In figure 13(*a*, *b*), the profiles of the streamwise amplitude for the splitter plate are compared for the case where the turbulent intensity profiles are still developing downstream ($\Delta U = 3.3$ m/s, $r = 0.73$) and the case where the profiles are self-preserving ($\Delta U = 4.6$ m/s, $r = 0.61$). The noticeable difference between the two cases appears to be that the amplitude profiles have two peaks and decay with distance downstream in the former case. In the latter case, the initial double-peaked profile eventually disappears and evolves to have only a single peak further downstream. For the half-frame-screen experiment ($\Delta U = 7.08$ m/s, $r = 0.52$), the amplitude profiles are close to self-preserving, similar to the above latter case (figure 13*c*).

For the transverse amplitude, the profiles do not show any double-peaked appearance (figures 14*a–c*). In fact, they are relatively uniform when compared to their turbulent-intensity profiles (figure 5). Similarly to the streamwise component, the amplitude profiles for the transverse component are nearly self-preserving for the shear layers that are self-preserving.

Figure 15(*a–d*) shows the evolution of the centreline ($\eta = 0$) oscillation amplitude for the shear layers generated from the splitter plate and the half-frame screen with the streamwise coordinate $(x_1 - x_0)$. For the splitter-plate experiments (figure 15*a* and *c*), the local fundamental amplitudes $\langle A_1\rangle/\Delta U$ and $\langle A_2\rangle/\Delta U$ grow initially corresponding to the initial roll-up near the origin and achieve maximum values. This process is followed by a gradual decay until they reach the asymptotic values of about 0.14 and 0.06, for the streamwise and transverse components respectively. These asymptotic values obtained are independent of initial conditions (in the present experiments) imposed at the splitter plate such as the initial momentum thickness, boundary-layer conditions or the velocity ratio r.

For the half-frame-screen experiments, the evolution of the amplitude of the local fundamental-mode oscillation is quite different. This trend may be attributed to some differences in the initial conditions and the experimental apparatus. In the half-frame experiments, the shear layer contains three-dimensional small-scale fluctuations well before the large-scale vortices are formed, very weak initially. However, the mechanism that generates the vortex elements should be essentially the same as the splitter-plate experiments. Despite the differences in the initial conditions, the asymptotic amplitudes $\langle A_1/\Delta U\rangle$ and $\langle A_2/\Delta U\rangle$ are found to settle at about 0.14 and 0.06, which are the same as for the splitter-plate experiments.

5.4. *Oscillation frequency*

The choice for L as the shear-layer lengthscale used in the present study is based on the fact that it is measured directly, the reasonable success of representing the mean velocity profile as $\frac{1}{2}(1+\mathrm{erf}(a\eta))$, where $\eta \equiv x_2 - x_{2c}/L$, and more importantly it allows

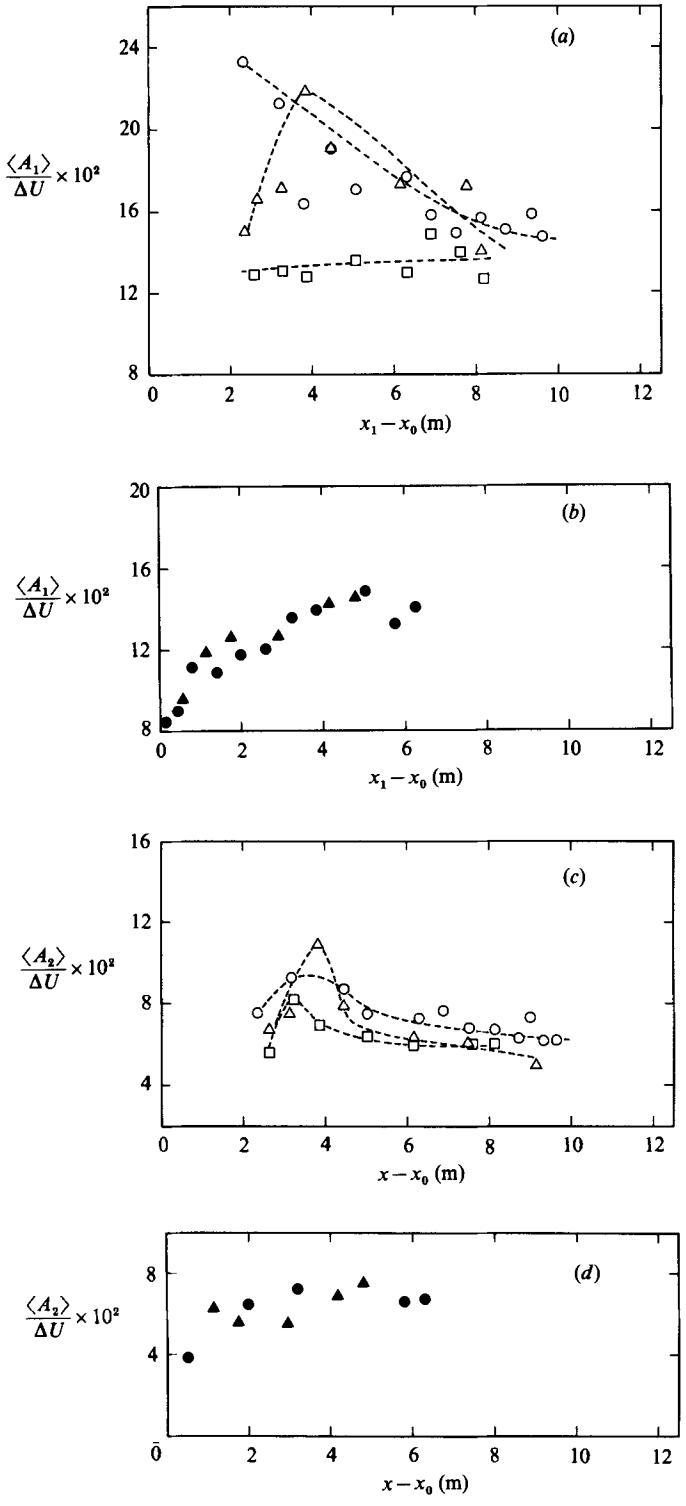

FIGURE 15. Evolution of the amplitude at the centreline of the shear layers. Splitter-plate experiments: △, $\Delta U = 3.3$ m/s; ○, 4.0 m/s; □, 4.6 m/s. Half-frame-screen experiments: ●, $\Delta U = 7.08$ m/s; ▲, 5.05 m/s. (*a*), (*b*) Streamwise component; (*c*), (*d*) transverse component.

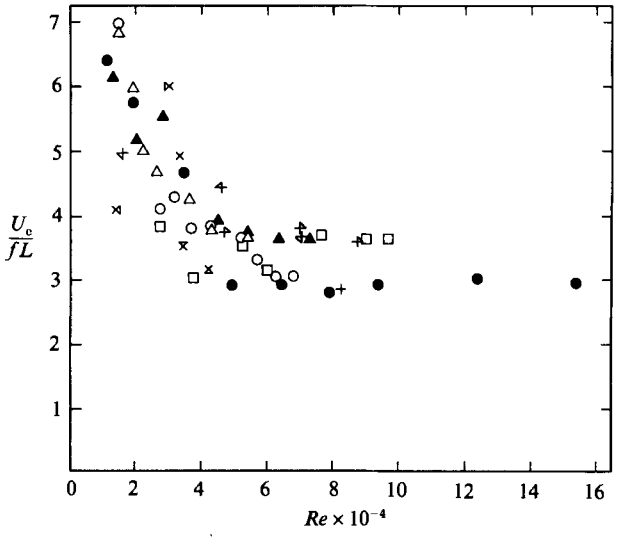

FIGURE 16. The inverse of the non-dimensional Strouhal number ($St = fL/U_c$) *vs.* local Reynolds number (Re). The symbols are the same as in figure 15 for the present data. Other symbols are ⊹, Spencer & Jones (1971); +, Wygnanski & Fiedler (1970); ×, Winant & Browand (1974); ⋉, Pui & Garthshore (1978); ⋊, Koochesfahani *et al.* (1979); ⋋, Dimotakis & Brown (1976); ⊹, Tavoularis & Corrsin (1981); ⋇, Jimenez (1983); ⊹, Jones *et al.* (1973).

one to compare the present data with previous data of other investigators. The lengthscale L is directly related to the vorticity thickness

$$\delta_\omega \equiv \Delta U / \frac{\mathrm{d}U_1}{\mathrm{d}y} \quad \text{as} \quad \delta_w = \tfrac{1}{2}\pi^{\frac{1}{2}} L = 0.974L, \tag{15}$$

where $a = 1.82$, if one assumes that the mean velocity profile can be approximated by the error function.

The fundamental frequency is normalized in terms of the local lengthscale L and the relative velocity between the structure convection velocity U_c and the velocity of the flow virtual origin U_0 as $fL/(U_c - U_0)$. Here f is the observed frequency in the reference frame moving at the velocity U_0. The dimensionless Strouhal number obtained is then Galilean invariant if the frequency and the relative convection velocity are measured in the same reference frame. In the present shear layers, as well as in others, the virtual origin can be defined to be the intersection of the loci of x_{2H}/h and x_{2L}/h, which is fixed relative to the fixed laboratory frame. The Strouhal number then reduces to fL/U_c, where f is now the measured frequency in the laboratory coordinate. The convection velocity of the large-scale structure is taken to be the average velocity difference between the two streams, on the basis of the flow visualization of Brown & Roshko (1974). It should be noted that the mean local convection velocity is not necessarily equal to the average velocity difference between the two stream (Jones *et al.* 1973); it is dependent on the transverse coordinate. However, at the shear-layer centreline, the assumed convection velocity is nearly equal to the local mean velocity where the frequency is also taken from this position. The appropriate lengthscale for the shear layer is taken to be its local value at the measurement station. This scale is also nearly the same as the average size of the structure whose properties are being examined. The inverse local fundamental Strouhal number U_c/Lf is shown and plotted as a function of the local Reynolds

number $Re = \Delta UL/\nu$ in figure 16. Also included in this figure are data of previous investigators, including both air and water as the working fluids. This plot suggests that the local Strouhal number, St, is dependent on the local Reynolds number, at least initially where the flow is in the developing state. If it is interpreted as the lengthscale ratio between the streamwise and the transverse directions, figure 16 shows the relaxation of the structure spacing and the structure size ratio to the asymptotic value. The data suggest that it varies between 3 and 4. The mechanisms for this relaxation are the large-scale structure fusions, which are discrete and random in both space and time, as well as the growth of its size as a result of engulfing the irrotational fluid.

The scatter of St in the present study is quite large, but comparable with other studies. This does not imply experimental inaccuracies of other investigators. Both L and f were obtained graphically from previous reports and are in a sense random variables. However, the trend is clear. It should be noted that previously St was thought to be constant (Dimotakis & Brown 1976; Winand & Browand 1974) and independent of Re.

6. Summary

In the present study, the shear layers were generated from a common splitter plate as well as from the half-frame-screen apparatus. For the shear layers, which are self-preserving from both types of apparatus, the mean velocity profiles, the maximum turbulent intensities at the centreline and the large-scale structure amplitudes are asymptotically equal. The orientation of the structure appears to be tilting backward on the high-speed side. For the shear layers that are still in developing state, the large-scale structure amplitudes also asymptote to nearly the same values regardless of the generating devices even though the turbulent intensities are still evolving with the distance down-stream. A common feature of all the shear layers investigated is the initially strong dependence of the local St on Re.

This work is supported by the Office of Naval Research, Fluid Dynamic Program. The author wishes to acknowledge helpful discussions with the late Professor Stan Corrsin and also with Drs J. Brasseur, S. Tavoularis, D. Walker and M. Walker. During the research, the author was a Postdoctoral fellow in the Department of Chemical Engineering, the John Hopkins University.

REFERENCES

Batt, R. G. 1975 Some measurement on the effect of tripping the two-dimensional shear layer. *AIAA J.* **13**, 245–247.

Batt, R. G. 1977 Turbulent mixing of passive and chemically reacting species in a low-speed shear layer. *J. Fluid Mech.* **82**, 53–95.

Bendat, J. S. & Piersol, A. G. 1971 *Random Data: Analysis and Measurement Procedures.* Wiley-Interscience.

Browand, F. K. 1966 An experimental investigation of the instability of an incompressible, separated shear layer. *J. Fluid Mech.* **26**, 281–307.

Browand, F. K. & Latigo, B. O. 1979 Growth of the two-dimensional mixing layer from a turbulent and non-turbulent boundary layer. *Phys. Fluids* **22**, 1011–1019.

Browand, F. K. & Troutt, T. R. 1980 A note on spanwise structure in the two-dimensional mixing layer. *J. Fluid Mech.* **97**, 771–781.

Browand, F. K. & Weidman, P. D. 1976 Large scales in the developing mixing layer. *J. Fluid Mech.* **76**, 127–144.

BROWN, G. L. & ROSHKO, A. 1974 On density effects in turbulent mixing layers. *J. Fluid Mech.* **64**, 775–816.

CANTWELL, B. & COLES, D. 1983 An experimental study of entrainment and transport in the turbulent near-wake of a circular cylinder. *J. Fluid Mech.* **136**, 321–374.

CHAMPAGNE, F. H., PAO, Y. H. & WYGNANSKI, I. J. 1976 On the two-dimensional mixing region. *J. Fluid Mech.* **74**, 209–250.

CHANDRSUDA, C., MEHTA, R. D., WEIR, A. D. & BRADSHAW, P. 1978 Effect of free-stream turbulence on large structure in turbulent mixing layers. *J. Fluid Mech.* **85**, 693–704.

COMTE-BELLOT, G. & CORRISIN, S. 1966 The use of a contraction to improve the isotropy of grid-generated turbulence. *J. Fluid Mech.* **25**, 657–682

COMTE-BELLOT, G. & CORRSIN, S. 1971 Simple Eulerian time correlations of full and narrow-band signals in grid-generated, 'isotropic' turbulence. *J. Fluid Mech.* **48**, 273–337.

CORRSIN, S. & KISTLER, A. 1955 Free stream boundaries of turbulent flows. *NACA Rep.* 1244.

DIMOTAKIS, P. E. & BROWN, G. L. 1976 The mixing layer at high Reynolds number: large-structure dynamics and entrainment. *J. Fluid Mech.* **78**, 535–560.

DZIOMBA, B. & FIEDLER, H. E. 1985 Effect of initial conditions on two-dimensional free shear layers. *J. Fluid Mech.* **152**, 419–422.

FREYMUTH, P. 1966 On transmission in a separated laminar boundary layer. *J. Fluid Mech.* **25**, 683–704.

GASTER, M., KIT, E. & WYGNANSKI, I. 1985 Large-scale structures in a forced turbulent mixing layer. *J. Fluid Mech.* **150**, 23–39.

GRANT, H. L. 1958 The large eddies of turbulent motion. *J. Fluid Mech.* **4**, 149–190.

HO, C.-M. & HUERRE, P. 1984 Perturbed free shear layers. *Ann. Rev. Fluid Mech.* **16**, 365–424.

HUSSAIN, A. K. M. F. 1983 Coherent structures–reality and myth. *Phys. Fluids* **26**, 2816–2850.

HUSSAIN, A. K. M. F. & REYNOLDS, W. C. 1970 The mechanics of an organized wave in turbulent shear flow. *J. Fluid Mech.* **41**, 241–258.

HUSSAIN, A. K. M. F. & ZEDAN, M. F. 1978*a* Effects of initial condition on the axisymmetric free shear layer: effect of the initial momentum thickness. *Phys. Fluids* **21**, 1100–1112.

HUSSAIN, A. K. M. F. & ZEDAN, M. F. 1978*b* Effects of initial condition on the axisymmetric free shear layer: effect of the initial fluctuation level. *Phys. Fluids* **21**, 1475–1481.

JIMENEZ, J. 1983 A spanwise structure in the plane shear layer. *J. Fluid Mech.* **132**, 319–336.

JIMINEZ, J., COGOLLOS, M. & BERNAL, L. 1985 A perspective view of the plane mixing layer. *J. Fluid Mech.* **152**, 125–143.

JONES, B. G., PLANCHON, H. P. & HEMMERSLEY, R. J. 1973 Turbulent correlation measurements in a two-stream mixing layer. *AIAA J.* **11**, 1146–1150.

KOOCHESFAHANI, M. M., CATHERASOO, C. J., DIMOTAKIS, P. E., GARIB, M. & LANG, D. B. 1979 Two-point LDV measurements in a plane mixing layer. *AIAA J.* **17**, 1347–1351.

LIEPMAN, H. W. & LAUFER, J. 1947 Investigations of free turbulent mixing. *NACA Tech. Note* 1257.

MIKSAD, R. 1972 Experiments on the non-linear stages of free-shear-layer transition. *J. Fluid Mech.* **56**, 695–719.

MIKSAD, R. 1973 Experiments on non-linear interactions in the transition of a free shear layer. *J. Fluid Mech.* **59**, 1–21.

MUMFORD, J. C. 1982 The structures of the large eddies in fully developed turbulent shear flows. Part I. The plane jet. *J. Fluid Mech.* **118**, 241–268.

OGUCHI, H. & INOUE, O. 1984 Mixing layer produced by a screen and its dependence on initial conditions. *J. Fluid Mech.* **142**, 217–231.

OSTER, D. & WYGNANSKI, I. 1982 The forced mixing layer between parallel streams. *J. Fluid Mech.* **123**, 91–130.

PATEL, R. R. 1973 An experimental study of a plane mixing layer. *AIAA J.* **11**, 67–71.

PAYNE, F. R. & LUMLEY, J. L. 1967 Large eddy structure of the turbulent wake behind a circular cylinder. *Phys. Fluids* **10**, S194–S196.

PHILLIPS, O. M. 1955 The irrotational motion outside a free turbulent boundary. *Proc. R. Phil. Soc. Lond.* **51**, 220–229.

PUI, N. K. & GARTSHORE, I. S. 1979 Measurements of the growth rate and structure in plane turbulent mixing layers. *J. Fluid Mech.* **91**, 111–130.

ROSHKO, A. 1954 On the development of turbulent wakes from vortex streets. *NACA Tech. Note* 1163.

SPENCER, B. W. & JONES, B. G. 1971 Statistical investigation of pressure and velocity fields in the turbulent two-stream mixing layer. *AIAA Paper* 71-613.

SOKOLOV, M., HUSSAIN, A. K. M. F., KLEIS, S. J. & HUSAIN, Z. D. 1980 A turbulent spot in an axisymmetric free shear layer. Part 1. *J. Fluid Mech.* **98**, 65–95.

TAVOULARIS, S. & CORRSIN, S. 1981 The structure of a turbulent shear layer embedded in turbulence. A preprint manuscript.

TOWNSEND, A. 1976 *The Structure of Turbulent Flow.* Cambridge University Press.

WINANT, C. D. & BROWAND, F. K. 1974 Vortex pairing: the mechanism of turbulent mixing-layer growth at moderate Reynolds number. *J. Fluid Mech.* **63**, 237–255.

WYGNANSKI, I. & FIEDLER, H. E. 1970 The two-dimensional mixing region. *J. Fluid Mech.* **41**, 327–361.

WYGNANSKI, I., OSTER, D., FIEDLER, H. & DZIOMBA, B. 1979 On the perseverence of a quasi-two-dimensional eddy-structure in a turbulent mixing layer. *J. Fluid Mech.* **93**, 325–335.